Solution Conformation of the (−)-*trans*-*anti*-[BP]dG Adduct Opposite a Deletion Site in a DNA Duplex: Intercalation of the Covalently Attached Benzo[*a*]pyrene into the Helix with Base Displacement of the Modified Deoxyguanosine into the Minor Groove[†]

Binbin Feng,[‡] Andrey Gorin,[‡] Alexander Kolbanovskiy,[§] Brian E. Hingerty,[∥,⊥] Nicholas E. Geacintov,[§] Suse Broyde,[▽] and Dinshaw J. Patel*[,‡]

Cellular Biochemistry and Biophysics Program, Memorial Sloan Kettering Cancer Center, New York, New York 10021, Chemistry and Biology Departments, New York University, New York, New York 10003, Oak Ridge National Laboratory, Oak Ridge, Tennessee 37831, and Knox Computer Consultants, Knoxville, Tennessee 37923

Received January 13, 1997; Revised Manuscript Received August 28, 1997[⊗]

ABSTRACT: A combined NMR-computational approach was employed to determine the solution structure of the (−)-*trans*-*anti*-[BP]dG adduct positioned opposite a −1 deletion site in the d(C1-C2−A3-T4-C5-[BP]G6-C7-T8-A9-C10-C11)·d(G12-G13-T14-A15-G16-G17-A18-T19-G20-G21) sequence context. The (−)-*trans*-*anti*-[BP]dG moiety is derived from the binding of the (−)-*anti*-benzo[*a*]pyrene diol epoxide [(−)-*anti*-BPDE] to N^2 of dG6 and has a 10*R* absolute configuration at the [BP]dG linkage site. The exchangeable and non-exchangeable protons of the benzo[*a*]pyrenyl moiety and the nucleic acid were assigned following analysis of two-dimensional NMR data sets in H_2O and D_2O solution. The solution conformation has been determined by incorporating intramolecular and intermolecular proton−proton distances defined by lower and upper bounds deduced from NOESY spectra as restraints in molecular mechanics computations in torsion angle space followed by restrained molecular dynamics calculations based on a NOE distance and intensity refinement protocol. Our structural studies establish that the aromatic BP ring system intercalates into the helix opposite the deletion site, while the modified deoxyguanosine residue is displaced into the minor groove with its face parallel to the helix axis. The intercalation site is wedge-shaped and the BP aromatic ring system stacks over intact flanking Watson−Crick dG·dC base pairs. The modified deoxyguanosine stacks over the minor groove face of the sugar ring of the 5′-flanking dC5 residue. The BP moiety is positioned with the benzylic ring oriented toward the minor groove and the distal pyrenyl aromatic ring directed toward the major groove. This conformation strikingly contrasts with the corresponding structure in the full duplex with the same 10*R* (−)-*trans*-*anti*-[BP]dG lesion positioned opposite a complementary dC residue [de los Santos et al. (1992) *Biochemistry 31*, 5245−5252); in this case the aromatic BP ring system is located in the minor groove, and there is no disruption of the [BP]dG·dC Watson−Crick base pairing alignment. The intercalation−base displacement features of the 10*R* (−)-*trans*-*anti*-[BP]dG adduct opposite a deletion site have features in common to those of the 10*S* (+)-*trans*-*anti*-[BP]dG adduct opposite a deletion site previously reported by Cosman et al. [(1994)(*Biochemistry 33*, 11507−11517], except that there is a nearly 180° rotation of the BP residue about the axis of the helix at the base-displaced intercalation site and the modified deoxyguanosine is positioned in the opposite groove. In the 10*S* adduct, the benzylic ring is in the major groove and the aromatic ring systems point toward the minor groove. This work extends the theme of opposite orientations of adducts derived from chiral pairs of (+)- and (−)-*anti*-BPDE enantiomers; both 10*S* and 10*R* adducts can be positioned with opposite orientations either in the minor groove or at base displaced intercalation sites, depending on the presence or absence of the partner dC base in the complementary strand.

The relationships between the structures of polycyclic aromatic hydrocarbon (PAH) carcinogens and their biological activities have long been of great interest to chemists and biologists [reviewed in Singer and Grunberger (1983) and Harvey (1991)]. Benzo[*a*]pyrene (BP), like other PAH compounds, is metabolized to highly reactive, mutagenic and tumorigenic bay region diol epoxide derivatives [reviewed in Conney (1982)]. The most tumorigenic derivative of BP is (+)-7*R*,8*S*-dihydroxy-9*S*,10*R*-epoxy-7,8,9,10-tetrahydrobenzo[*a*]pyrene [(+)-*anti*-BPDE], while the (−)-7*S*,8*R*,9*R*,10*S*-enantiomer [(−)-*anti*-BPDE] is inactive in the mouse model system (Buening et al., 1978; Slaga et al., 1979). The mutagenic activities of these two chiral compounds are also strikingly different from one another (Wood et al., 1977; Brookes & Osborne et al., 1982; Wei et al., 1994; Moriya et al., 1996). Differences in the chemical reactivities of these two *anti*-BPDE enantiomers with native DNA (Meehan & Straub, 1979; Cheng et al., 1989), and the conformations of

[†] This research is supported by NIH Grant CA-46533 to D.J.P., by NIH Grant CA-20851 and DOE Grant DE-FG02-88ER60405 to N.E.G., by NIH Grant CA-28038, NIH Grant RR-06458, and DOE Grant DE-FG02-90ER60931 to S.B., and by DOE Contract DE-AC05-840R21400 with Martin-Marietta Energy Systems and DOE OHER Field Work Proposal ERKP931 to B.E.H.

* Corresponding author.
[‡] Memorial Sloan Kettering Cancer Center.
[§] Chemistry Department, NYU.
[∥] Oak Ridge Nation Laboratory.
[⊥] Knox Computer Consultant.
[▽] Biology Department, NYU.

[⊗] Abstract published in *Advance ACS Abstracts,* November 1, 1997.

S0006-2960(97)00070-6 CCC: $14.00 © 1997 American Chemical Society

the adducts formed (Cosman et al., 1992; de los Santos et al., 1992; Fountain & Krugh, 1995; Schurter et al., 1995; Zegar et al., 1996b) may play critical roles in the expression of the mutagenic potentials of these two *anti*-BPDE enantiomers.

Both (+)- and (−)-*anti*-BPDE react chemically with DNA by binding predominantly to the exocyclic amino groups of the two purines. The major adducts arise from either *trans* or *cis* addition of the N^2 group of deoxyguanosine to the C^{10} position of BPDE (Meehan & Straub, 1979; Cheng et al., 1989). Thus, there are four different stereoisomeric [BP]-dG adducts (Figure S1, Supporting Information), two each with 10*S* absolute configuration at the covalent linkage site [abbreviated as (+)-*trans-anti*- and (−)-*cis-anti*-[BP]-N^2-dG], and two with 10*R* stereochemistry [(−)-*trans-anti*- and (+)-*cis-anti*-[BP]-N^2-dG]. While these four stereoisomeric adducts are formed in different proportions in native DNA (Cheng et al., 1989), the biological response to these adducts may be more a function of the structural properties of these lesions than their relative abundance. As a first step toward establishing structure−activity relationships, we have determined the conformations of these four [BP]dG lesions positioned opposite dC in the same d(C-[BP]G-C)·d(G-C-G) sequence context at the 11-mer DNA duplex level using NMR techniques and molecular mechanics computations (Cosman et al., 1992, 1993a, 1996; de los Santos et al., 1992).

These four stereoisomeric [BP]dG adducts when positioned opposite dC are characterized by a remarkable diversity of conformations which depend on the 10*S* or 10*R* stereochemistry, and to a lesser extent, on the absolute configurations of the OH groups about the C^7, C^8, and C^9 chiral carbon centers. The enantiomeric pairs of PAH diol epoxides give rise to opposite orientations of the adducted polycyclic aromatic residues relative to the modified dG residues. The pyrenyl residues in both the 10*S* (+)-*trans-anti*- and the 10*R* (−)-*trans-anti*-[BP]dG adducts opposite dC are positioned in the minor groove, pointing oppositely, toward the 5′- or 3′-ends of the modified strand, respectively (Cosman et al., 1992; de los Santos et al., 1992). In the 10*R* (+)-*cis-anti*- and the 10*S* (−)-*cis-anti*-[BP]dG adducts opposite dC on the other hand, the pyrenyl residues are inserted intercalatively into the double helix, and displace the modified deoxyguanosine bases into the minor and major grooves, respectively (Cosman et al., 1993a,1996). The pyrenyl residues are oppositely oriented at these intercalation sites via a 180° rotation about the helix axis: in the 10*R* (+)-*cis-anti*-[BP]dG adduct, the benzylic ring is situated within the minor groove and the pyrenyl ring system points toward the major groove, while in the 10*S* (−)-*cis-anti*-[BP]-dG adduct, the benzylic ring is in the major groove and the aromatic ring system points toward the minor groove side of the double helix.

The base or lack of it opposite the [BP]dG adduct site can also exhibit striking effects on the observed adduct conformations. We have studied the effects of deleting the partner base dC opposite the 10*S* (+)-*trans-anti*-[BP]dG adduct (Cosman et al., 1994a) and the 10*R* (+)-*cis-anti*-[BP]-dG adduct (Cosman et al., 1994b) within the d(C-[BP]G-C)·d(G-G) sequence context at the 11/10-mer duplex level. This type of sequence models the situation following mutagenic replication in which the damaged base has been skipped by the replication machinery, resulting in a −1 deletion mutation in the nascent DNA strand. Both structures

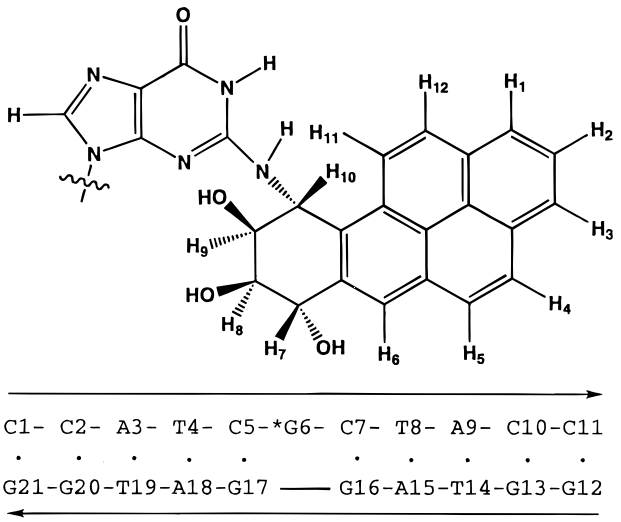

FIGURE 1: (A) Chemical structure of the (−)-*trans-anti*-[BP]dG adduct. (B) Sequence of the 11/10-mer containing a (−)-*trans-anti*-[BP]dG adduct at the *G6 position.

involve intercalation of the pyrenyl ring into the helix but differ in that the modified deoxyguanosine is base displaced into the major groove for the (+)-*trans-anti*-[BP]dG opposite a −1 deletion site (Cosman et al., 1994a) and into the minor groove for the (+)-*cis-anti*-[BP]dG opposite a −1 deletion site (Cosman et al., 1994b). The present study extends this research to the structural characterization of the 10*R* (−)-*trans-anti*-[BP]dG lesion (Figure 1A) opposite a −1 deletion site in the same d(C-[BP]G-C)·d(G-G) sequence context at the 11/10-mer (Figure 1B) level. Such a comparative study should define the relative contribution of chirality at the C^{10} linkage site and at the remaining C^7, C^8, and C^9 chiral centers of the benzylic ring to the structure of stereoisomeric [BP]-dG adducts positioned opposite a −1 deletion site.

MATERIALS AND METHODS

Preparation of the (−)-trans-anti-[BP]dG·del 11/10-Mer. Racemic *anti*-BPDE was purchased from the National Cancer Institute Chemical Carcinogen Reference Standard Repository. The synthesis of the [BP]dG covalent adduct in the d(C-C-A-T-C-[BP]G-C-T-A-C-C) sequence was carried out starting from racemic *anti*-BPDE using previously described methods (Cosman et al., 1990). The (−)-*trans-anti*-[BP]-dG containing 11-mer was separable from the (+)-*trans-anti*, (−)-*cis-anti*, and (+)-*cis-anti* isomeric adducts by preparative HPLC on a C18 ODS Hypersil column (Cosman et al., 1990). The modified enantiomerically pure d(C-C-A-T-C-[BP]G-C-T-A-C-C) 11-mer strand was annealed to the complementary unmodified d(G-G-T-A-G-G-A-T-G-G) 10-mer strand at 70 °C, and the stoichiometry was followed by monitoring single proton resonances in both strands. The NMR spectra of the (−)-*trans-anti*-[BP]dG·del 11/10-mer (approximately 8 mg) were recorded in 0.5 mL of 0.1 M NaCl, 0.01 M phosphate, and 0.1 mM Na_2EDTA at pH 7.0.

NMR Experiments. All experiments were recorded on Varian Unity Plus 500 and 600 MHz NMR spectrometers. The details of NMR data collection and analysis are the same as outlined in the Methods section of the accompanying paper (Feng et al., 1997). Distance restraints were deduced from a NOESY (mixing time of 100 ms) data set recorded in H_2O at 1 °C and from NOESY (mixing times of 50, 90, 130,

170, and 300 ms) buildup set in D_2O on the adduct 11/10-mer.

Molecular Mechanics Computations. Molecular mechanics calculations guided by NOE distance restraints were carried out with DUPLEX (Hingerty et al., 1989), along the lines outlined in the Methods sections of previous papers from our laboratory (Cosman et al., 1993a,b).

Relaxation Matrix Refinement. The final unrestrained energy minimized structure obtained during the first stage DUPLEX based calculations was used as the starting point for the second stage of refinement using X-PLOR (Brunger, 1992). The details of pseudoenergy function and the relaxation matrix refinement protocol are the same as outlined in the Methods sections of the accompanying paper (Feng et al., 1997).

The relaxation matrix was set up for the non-exchangeable protons; the exchangeable imino, amino and hydroxyl protons were exchanged for deuterons. A total of 932 intensities from the NOESY experiment in D_2O (233 intensities per mixing time) and 239 distance restraints were included in the calculations. Dihedral angle restraints (corresponding to B-DNA) were included with a very low weight of 5 kcal·rad^{-2} for four base pairs toward either duplex end with no dihedral angle restraints used for the central d(T4-C5-[BP]G6-C7-T8)·d(A15-G16-G17-A18) segment.

RESULTS

The thermal melting points (T_m) at optical concentrations (10 μM strand concentration) were reported to be 24 °C for the unmodified dG·del 11/10-mer control and 38 °C for the (−)-*trans-anti*-[BP]dG·del 11/10-mer (Ya et al., 1994). The observed stabilization of the (−)-*trans-anti*-[BP]dG·del 11/10-mer at ambient temperature allowed us to undertake a detailed NMR study of this system.

Exchangeable Nucleic Acid Proton Spectra. The exchangeable proton NMR spectrum (10.0−14.5 ppm) of the (−)-*trans-anti*-[BP]dG·del 11/10-mer duplex in H_2O buffer, pH 7.0, at 1 °C is plotted in Figure 2A. Three upfield-shifted imino protons (two of which are overlapped at 10.55 ppm) are detected in addition to resolved imino protons between 12.7 and 13.7 ppm.

These imino protons have been assigned by standard procedures [reviewed in Patel et al. (1987) and van de Ven and Hilbers (1988)] following analysis of the 100 ms mixing time NOESY spectrum (Figure 3). NOEs can be detected between adjacent imino protons from dG13 to dG16 and from dG17 to dG20 on either side of the [BP]dG6 lesion site. However, NOEs are not observed between the imino protons of dG16 and dG17 (boxed region, Figure 3A) on either side of the lesion site. Further, NOEs are not observed between the imino protons of [BP]dG and the imino protons of flanking dG16 and dG17 residues. It should be noted that the narrow imino protons of dG16 (11.41 ppm) and dG17 (10.55 ppm) have shifted dramatically to high field in the adduct 11/10-mer.

NOEs between the deoxyguanosine imino and deoxycytidine amino protons for the dC5·dG17 (peaks D, D′, Figure 3B) and the dC7·dG16 (peaks A, A′, Figure 3B) base pairs establish Watson−Crick pairing at these dG·dC base pairs adjacent to the lesion site. The deoxycytidine amino protons of dC7 (6.01, 6.88 ppm) and, to a lesser extent, dC5 (6.72, 7.40 ppm), are also shifted to high field in the adduct duplex. These large upfield shifts of the deoxyguanosine imino and deoxycytidine amino protons of the dC5·dG17 and dC7·dG16 base pairs suggest that the pyrenyl ring of [BP]dG6 intercalates into the helix between these base pairs in the adduct 11/10-mer.

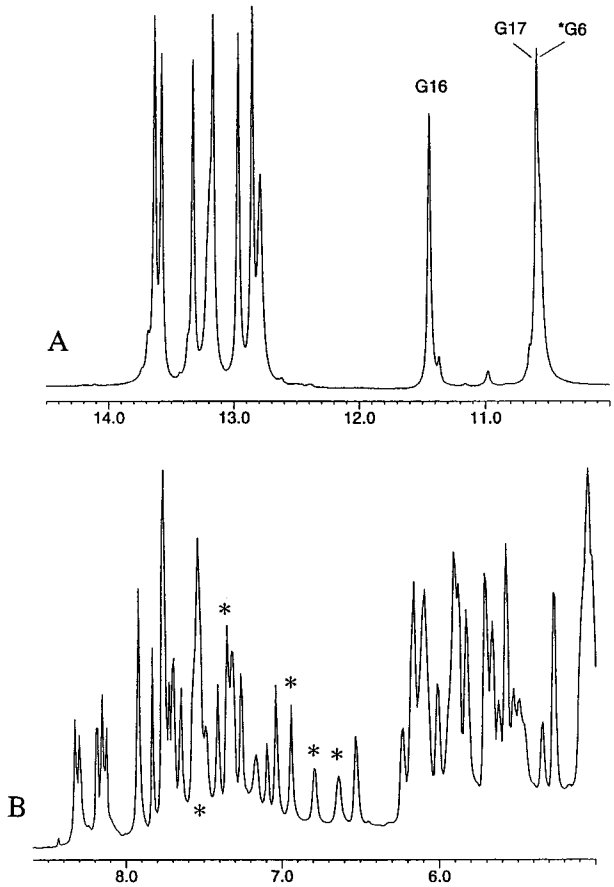

FIGURE 2: (A) Imino proton spectrum (10.0−14.5 ppm) in H_2O buffer at 1 °C and (B) non-exchangeable proton spectrum (5.0−8.6 ppm) in D_2O buffer at 20 °C of the (−)-*trans-anti*-[BP]dG·del 11/10-mer. The buffer was 0.1 M NaCl and 10 mM phosphate, aqueous solution at pH 7.0. The imino protons of *G6, dG16, and dG17 are assigned over spectrum A. The resolved pyrenyl non-exchangeable protons (some of which are overlapped with DNA protons) are designated by asterisks over the spectrum in B.

The imino proton of [BP]dG6 is also shifted upfield to 10.55 ppm where it overlaps with the imino protons of dG17 (Figure 2A). This upfield shift suggests that the modified deoxyguanosine is most likely displaced out of the helix following intercalation of the pyrenyl ring. The upfield chemical shift and broadening of its line width at elevated temperatures reflect exposure of the imino proton of [BP]-dG6 to solvent consistent with base displacement of the modified deoxyguanosine out of the helix. The corresponding amino proton of [BP]dG6 resonates at 6.41 ppm (peak C, Figure 3B) in the adduct 11/10-mer.

The exchangeable imino and amino proton chemical shifts for the central d(C5-[BP]G6-C7)·d(G16-G17) segment in the solution structure of the (−)-*trans-anti*-[BP]dG·del 11/10-mer at 1 °C are listed in Table 1. The exchangeable proton chemical shifts of the entire adduct duplex are listed in Table S1 (Supporting Information).

We observe resolved imino proton resonances between 10.5 and 11.5 ppm from a minor component (<10%) in the proton spectrum recorded in Figure 2A. This minor component is assigned to the (+)-*cis-anti*-[BP]dG adduct opposite

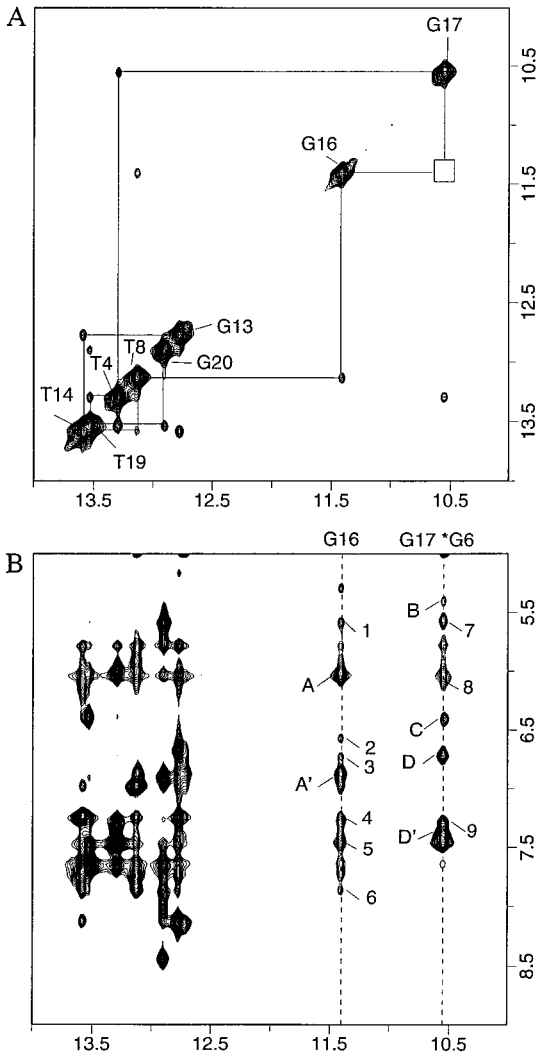

FIGURE 3: Expanded NOESY (100 ms mixing time) contour plots of the (−)-*trans-anti*-[BP]dG·del 11/10-mer in H_2O buffer at 1 °C. (A) NOE connectivities in the symmetrical 10.0−14.0 ppm region. The imino proton assignments are labeled along the diagonal. The lines trace the NOE connectivities between imino protons on adjacent base pairs starting at dG20 toward one end of the helix and proceeding to dG13 toward the other end of the helix. This connectivity tracing is broken between the imino protons of dG16 and dG17. (B) NOE connectivities between the imino protons (10.0−14.0 ppm) and the base and amino protons (5.0−9.0 ppm). The imino protons of [BP]dG6, dG16, and dG17 centered about the lesion site are labeled in the figure. The intramolecular cross-peaks A−D between nucleic acid protons are assigned as follows: (A,A′) G16(NH1)−C7(NH_2-4a,b); (B) [BP]G6(NH1)−C5(H1′); (C) [BP]G6(NH1)−[BP]G6(NH_2-2); (D,D′) G17(NH1)−C5(NH_2-4a,b). The intermolecular cross-peaks 1−9 are assigned as follows: (1) G16(NH1)-BP(H4); (2) G16(NH1)−BP(H5); (3) G16(NH1)−BP-(H3); (4) G16(NH1)−BP(H2/H12); (5) G16(NH1)−BP(H1); (6) G16(NH1)−BP(H6); (7) G17(NH1)−BP(H4); (8) [BP]G6(NH1)−BP(H10); (9) G17(NH1)−BP(H2/H12).

a −1 deletion site at the 11/10-mer level based on its distinct imino proton chemical shifts reported previously (Cosman et al., 1994b). The minor component has resulted from incomplete HPLC purification of the (−)-*trans-anti*-[BP]dG adduct containing 11-mer from the contaminating (+)-*cis-anti*-[BP]dG adduct containing 11-mer.

Non-Exchangeable Nucleic Acid Proton Spectra. The non-exchangeable base and sugar H1′ proton spectrum (5.0−8.6 ppm) of the (−)-*trans-anti*-[BP]dG·dC 11/10-mer in D_2O buffer, pH 7.0 at 20 °C is plotted in Figure 2B. The well-resolved proton resonances have permitted us to assign both

Table 1: Proton Chemical Shifts of the d(C5-[BP]G6-C7)·d(G16-G17) Segment of the (−)-*trans-anti*-[BP]dG·del 11/10-mer in Aqueous Buffer

	exchangeable proton chemical shifts (ppm) 1 °C		
	G(NH1)	G(NH_2-2)	C(NH_2-4)
dC5·dG17	10.55		6.72,[a] 7.40[b]
dC7·dG16	11.41		6.01,[a] 6.88[b]
[BP]dG6	10.55	6.41	

	non-exchangeable proton chemical shifts (ppm), 25 °C					
	H8/H6	H2/H5	H1′	H2′, H2″	H3′	H4′
dC5	7.15	5.61	5.45	2.54, 1.16	4.90	3.60
[BP]dG6	8.11		6.52	2.69, 3.43	5.09	4.74
dC7	7.52	5.33	4.17	1.78, 1.96	4.26	4.10
dG16	7.64		5.94	2.46, 2.49	5.03	4.44
dG17	7.91		5.48	2.55, 2.67	5.04	4.50

[a] Exposed amino proton. [b] Hydrogen-bonded amino proton.

the benzo[*a*]pyrenyl and DNA protons in the adduct duplex. An expanded NOESY contour plot (300 ms mixing time) correlating the base proton (6.3−8.4 ppm) with the sugar H1′ and H3′ protons (3.9−6.7 ppm) for the adduct 11/10-mer at 20 °C is plotted in Figure 4. The NOE connectivities between the base and its own and 5′-flanking sugar H1′ protons for the d(T4-C5-[BP]G6-C7-T8) segment of the modified 11-mer strand (solid line) and the d(A15-G16-G17-A18) segment of the 10−mer deletion containing strand (dashed line) have been traced in Figure 4. The NOEs between the adjacent residues are absent for the dC5-[BP]-dG6 step and weak for the dT4-dC5 step on the modified strand. Further, no NOE is detected between the H8 proton of [BP]dG6 and the H5 proton of dC7 at the purine (3′-5′) pyrimidine step indicative of a structural distortion centered about the lesion site in the adduct 11/10-mer.

NOEs detected between the base protons of [BP]dG6 and the minor groove sugar protons of dC5 in the adduct duplex define the orientation of the deoxyguanosyl ring of [BP]dG6 within the d(C5-[BP]G6-C7) segment. These include NOEs between the H8 proton of [BP]dG6 and the H4′ proton of dC5 (peak 1, Figure S2, Supporting Information) and between the imino proton of [BP]dG6 and the H1′ proton of dC5 (peak B, Figure 3B). These results suggest that the deoxyguanosine of [BP]dG6 is displaced out of the helix into the minor groove and is oriented toward the 5′-end of the modified strand in the adduct 11/10-mer.

The non-exchangeable base and sugar proton chemical shifts have been assigned following analysis of the complete NOESY, DQF-COSY, and TOCSY data sets of the adduct 11/10-mer based on standard nucleic acid assignment procedures [reviewed in van de Ven and Hilbers (1988)]. The proton chemical shift values for the d(C5-[BP]G6-C7)·d(G16-G17) segment of the (−)-*trans-anti*-[BP]dG·dC 11/10-mer duplex at 20 °C are listed in Table 1. The non-exchangeable proton chemical shift assignments for the entire adduct duplex are listed in Table S1 (Supporting Information). It should be noted that several base and sugar proton resonances of the d(C5-[BP]G6-C7) segment in the adduct duplex exhibit unusual chemical shifts reflecting ring current contributions from nearby aromatic ring systems. The H2″ (1.16 ppm) and H4′ (3.60 ppm) protons of C5 and the H1′ (4.17 ppm) proton of C7 are shifted to high field while the H1′ (8.11 ppm) and H2" (3.43 ppm) protons of [BP]dG6 are shifted to low field in the adduct 11/10-mer (Table 1).

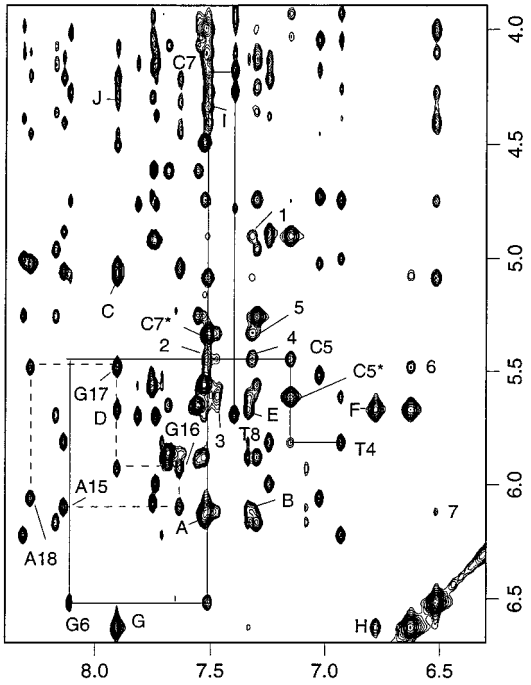

FIGURE 4: Expanded NOESY (300 ms mixing time) contour plot of the (−)-*trans-anti*-[BP]dG·del 11/10-mer in D_2O buffer at 20 °C establishing distance connectivities between the base (purine H8 and pyrimidine H6) protons (6.3−8.4 ppm) and the sugar H1′ and H3′ and deoxycytidine H5 protons (3.9−6.7 ppm). The NOE connectivities between the base and their own and 5′-flanking sugar H1′ protons from dT4 to dT8 on the modified strand are shown by solid lines and from dA15 to dA18 on the unmodified strand are shown by dashed lines. The assignments label the base to their own sugar H1′ NOEs while the deoxycytidine H6-H5 NOEs are designated by asterisks. Note the unusual upfield shift of the H1′ proton of dC7 and to a lesser extent the upfield shift of H5 proton of dC7 and the downfield shift of the H1′ proton of [BP]dG6. Note that the cross-peak linking the dC5-[BP]dG6 step is missing while the cross-peak linking the dT4-dC5 steps is weak. The intramolecular cross-peaks A−J between benzo[*a*]pyrene protons are assigned as follows: (A) BP(H10)−BP(H11); (B) BP(H10)−BP(H12); (C) BP(H6)−BP(H7); (D) BP(H4)−BP(H6); (E) BP(H2)−BP(H4); (F) BP(H3)−BP(H4); (G) BP(H5)−BP(H6); (H) BP(H3)−BP(H5); (I) BP(H9)−BP(H11); (J) BP(H6)−BP(H8). The intermolecular cross-peaks 1−7 are assigned as follows: (1) C5(H3′)−BP(H12); (2) C5(H1′)−BP(H11); (3) C5(H5)−BP(H1); (4) C5-(H1′)−BP(H12); (5) C7(H5)−BP(H12); (6) G17(H1′)−BP(H5); (7) G6(H1′)−BP(H10). The chemical shift values for the benzylic protons are BP(H7), 5.08 ppm; BP(H8), 4.07 ppm; BP(H9), 4.34 ppm; BP(H10), 6.12 ppm. The chemical shift values for the pyrenyl protons are BP(H11), 7.51 ppm; BP(H12), 7.32 ppm; BP(H1), 7.47 ppm; BP(H2), 7.34 ppm; BP(H3), 6.78 ppm; BP(H4), 5.66 ppm; BP(H5), 6.62 ppm; BP(H6), 7.91 ppm.

Non-Exchangeable Benzo[a]pyrenyl Protons. The benzylic and pyrenyl ring protons of [BP]dG6 have been assigned following analysis of the through space and through bond connectivities involving these protons in the (−)-*trans-anti*-[BP]dG·dC 11/10-mer duplex. The chemical shifts are listed in the caption to Figure 4 and are plotted (represented by closed circles) in Figure 5. The majority of the pyrenyl protons are shifted to high field with the largest upfield shifts detected at the H3 (6.78 ppm), H4 (5.66 ppm), and H5 (6.62 ppm) protons in the adduct 11/10-mer.

Intermolecular NOEs. A number of intermolecular NOEs between the exchangeable and non-exchangeable nucleic acid protons and the non-exchangeable BP protons have been identified and assigned in the NOESY spectrum of the (−)-*trans-anti*-[BP]dG·del 11/10-mer. Several of these intermolecular NOEs are labeled in the expanded NOESY contour plot of the exchangeable protons in H_2O solution (Figure 3B) and in the expanded NOESY contour plot of the non-exchangeable protons in D_2O solution (Figure 4) with the cross-peak assignments listed in the figure captions. Fourteen intermolecular NOEs defined by lower and upper bounds for the central d(C5-[BP]G6-C7)·d(G16-G17) segment that were used to guide the computations are listed in Table S2 (Supporting Information). Another nine weak intermolecular NOEs that were observed but not used in the computations are listed in Table S3 (Supporting Information).

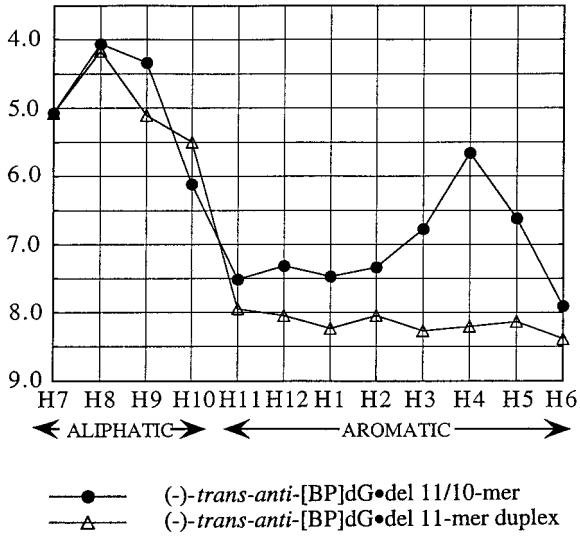

FIGURE 5: Plot comparing the benzo[*a*]pyrenyl ring proton chemical shifts in the (−)-*trans-anti*-[BP]dG·dC 11-mer duplex (△) and the (−)-*trans-anti*-[BP]dG·del 11/10-mer (●). The benzylic protons (H7, H8, H9, H10) are on the left, and the pyrenyl protons (H11, H12, H1, H2, H3, H4, H5, H6) are on the right of this plot.

The distribution of the observed intermolecular NOEs readily provides insights into the alignment of the intercalated pyrenyl ring relative to the d(C5-[BP]G6-C7) modified and d(G16-G17) deletion containing strands of the adduct duplex. We observe NOEs between the H3, H4, H5, and H6 protons of the BP pyrenyl ring and the imino and sugar H1′ protons of the d(G16−G17) deletion containing strand (Tables S2 and S3). We also observe NOEs between the H10, H11, H12, and H1 protons of the other long edge of the pyrenyl ring and the base and sugar protons of the d(C5-[BP]G6-C7) modification containing strand (Tables S2 and S3). The benzylic ring is likely to be positioned in the minor groove based on the observed NOE between the benzylic BP(H10) and the minor groove C7(H1′) protons (Table S3) while the farthest pyrenyl ring is positioned in the major groove based on the observed NOE between the pyrenyl BP(H1) and the major groove C5(H5) protons (Table S2). These intermolecular NOEs suggest an orthogonal alignment of the long axis of the pyrenyl ring and the long axis of the flanking base pairs at the intercalation site in the adduct 11/10-mer.

Phosphorus Spectra. Two phosphorus resonances are shifted to low field and two others are shifted to high field of the central cluster of phosphorus resonances in the spectrum of the (−)-*trans-anti*-[BP]dG·del 11/10-mer in D_2O at 20 °C (Figure S3A, Supporting Information). The phosphorus resonances in the adduct 11/10-mer spectrum have been assigned following analysis of the proton−phosphorus correlation contour plot recorded at 20 °C (Figure S3B, Supporting Information). The most downfield-shifted

phosphorus is assigned to the d(C5-[BP]G6) step while the most upfield-shifted phosphorus is assigned to the d([BP]-G6-C7) step on the modified strand of the adduct 11/10-mer.

The proton and phosphorus chemical shift values, as well as the magnitude of the through-space intramolecular and intermolecular NOE patterns between the proton pairs, are strikingly similar in the (+)-*cis-anti*-[BP]dG adduct (Cosman et al., 1994b) and the (−)-*trans-anti*-[BP]dG adduct (this study) positioned opposite −1 deletion sites.

Molecular Mechanics Computations. In the first stage of the calculations, we employed the DNA conformation reported previously for the solution structure of the central d(T4-C5-[BP]G6-C7-T8)·d(A15-G16-G17-A18) segment of the (+)-*cis-anti*-[BP]dG·del 11/10-mer (Cosman et al., 1994b) as the starting DNA structure. The (−)-*trans-anti*-[BP]-dG orientation space within the d(T4-C5-[BP]G6-C7-T8)·d(A15-G16-G17-A18) segment was then searched with sixteen energy minimization trials with DUPLEX. In these trials, the linkage torsional angles α' (dG6(N^1)-dG6(C^2)-dG6-(N^2)-BP(C^{10})) and β' (dG6(C^2)-dG6(N^2)-BP(C^{10})-BP(C^9)) were each started at 0°, 90°, 180°, and 270° in all combinations. In these trials, the benzylic ring was fixed in the distorted half-chair conformation with BP(H9) and BP(H10) in pseudoequatorial orientations and BP(H7) and BP(H8) in pseudoaxial orientations (Neidle et al., 1982) consistent with the NMR coupling constant data on the adduct 11/10-mer. The experimental coupling cross-peak patterns for the benzylic protons and their simulated counterparts show good agreement for proton−proton coupling constant values of ^3J(H7,H8) = 9.5 ± 0.5 Hz, ^3J(H8,H9) = 3.0 ± 0.5 Hz, and ^3J(H9,H10) = 3.5 ± 0.5 Hz.

The sixteen computed conformations of the d(T4-C5-[BP]-G6-C7-T8)·d(A15-G16-G17-A18) segment yielded a five-membered family of closely related structures with low energy and goodness-of-fit indices. A superpositioned view of the d(T4-C5-[BP]G6-C7-T8)·d(A15-G16-G17-A18) segment of these five structures is plotted in Figure S4 (Supporting Information). The d(T4-C5-[BP]G6-C7-T8)·d(A15-G16-G17-A18) segment of the lowest energy structure was employed in building the (−)-*trans-anti*-[BP]dG·del 11/10-mer. Subsequently, the hydrogen-bond penalty function and the distance restraints were released with energy minimization in one step, yielding an unrestrained minimum energy conformation of the (−)-*trans-anti*-[BP]dG·del 11/10-mer (Figure S5, Supporting Information). This structure was then employed in the second stage relaxation matrix refinement as described in Materials and Methods section.

Relaxation Matrix Refinement. An ensemble of six structures obtained during intesity refinment demonstrated an improved correspondence with experimental intensity and distance restraint data sets. The number of NOE distances violated by more than 0.2 Å decreased from 24 to 6 (with almost no violations in the central d(T4-C5-[BP]G6-C8-T8)·d(A15-G16-G17-A18) segment), and the NMR $R_{1/6}$-factor improved from an initial value of 7% to 4% (Table 2). All structures exhibit good stereochemistry with the rmsd values for bond length, bond angle, and improper dihedral angle violations of 0.01 ± 0.001 Å, 2.62 ± 0.05°, and 0.34 ± 0.03°, respectively.

The rmsd of all heavy atoms between the six structures and the initial structure is 2.67 ± 0.48 Å for all heavy atoms and 1.74 ± 0.10 Å for the central d(T4-C5-[BP]G6-C7-T8)·d(A15-G16-G17-A18) segment. At the same time the six structures exhibit good convergence properties. The pairwise rmsd in the set is 1.92 ± 0.40 Å for all heavy atoms and 1.17 ± 0.10 Å for the heavy atoms of the central d(T4-C5-[BP]G6-C7-T8)·d(A15-G16-G17-A18) segment (Table 2).

Table 2: NMR Refinement Statistics for the (−)-*trans-anti*-[BP]dG·del 11/10-Mer

NMR restraints	
total number of NOE intensities	233 per mixing time
NOE intensities in the central 5/4-mer region[a]	95 per mixing time
total number of NOE distances	239
NOE distances in the central 5/4-mer region[a]	96
structure statistics	
NMR $R_{1/6}$-factor	0.045 ± 0.001
rmsd of NOE violations	0.054 ± 0.005
number of NOE violations >0.2 Å	6.0 ± 2.4
number of NOE violations >0.2 Å in the central 5/4-mer region[a]	1.3 ± 0.5
deviations from the ideal geometry	
bond length (Å)	0.01 ± 0.001
bond angle (deg)	2.62 ± 0.05
impropers (deg)	0.34 ± 0.03
pairwise rmsd (Å) among the six refined structures (heavy atoms only)	
entire 11/10-mer	1.92 ± 0.40
central 5/4-mer region[a]	1.17 ± 0.13
central 5/4-mer region without backbone	0.87 ± 0.18

[a] The d(T4-C5-[BP]G6-C7-T8)·d(A15-G16-G17-A18) segment.

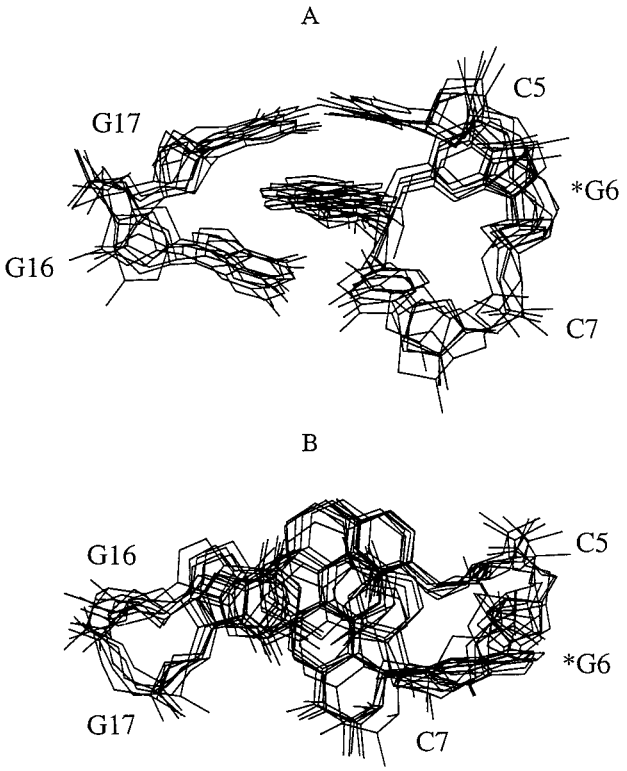

FIGURE 6: Superposition of the six relaxation matrix refined structures of the (−)-*trans-anti*-[BP]dG·del 11/10-mer. (A) View looking into the minor groove and normal to the helix axis of the d(C5-[BP]G6-C7)·d(G16-G17) segments. (B) View looking down the helix axis of the d(C5-[BP]G6-C7)·d(G16-G17) segments.

The corresponding superpositioned view of the six conformations of the d(C5-[BP]G6−C7)·d(G16-G17) segment is plotted in Figure 6A. A view looking down the helix axis of this segment in the six superpositioned conformations is plotted in Figure 6B.

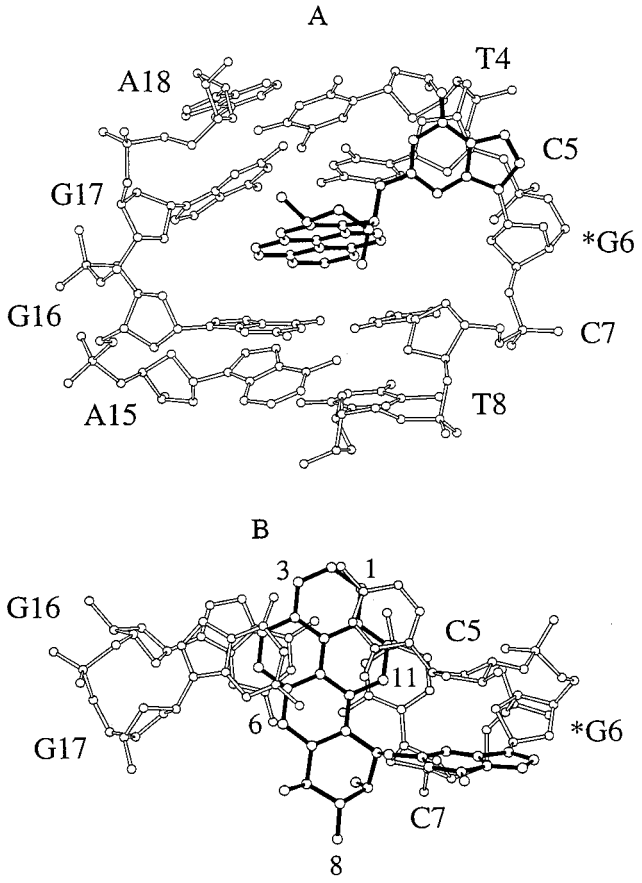

FIGURE 7: (A) View looking into the minor groove and normal to the helix axis for the d(T4-C5-[BP]G6-C7-T8)·d(A15-G16-G17-A18) segment in the representative structure of the (−)-*trans-anti*-[BP]dG·del 11/10-mer from the ensemble of six relaxation matrix refined structures. The BP ring is intercalated between the dC5·dG17 and dC7·dG16 base pairs which form a wedge-shaped intercalation site. The modified dG6 base is displaced into the minor groove and is directed toward the 5′-neighbor dC5 in the sequence. (B) View looking down the helix axis for the d(C5-[BP]G6-C7)·d(G16-G17) segment in the representative structure of the (−)-*trans-anti*-[BP]dG·del 11/10-mer from the ensemble of six relaxation matrix refined structures. The benzylic ring is positioned in the minor groove while the pyrenyl ring stacks over the Watson−Crick hydrogen bonding regions of the flanking dC5·dG17 and dC7·dG16 base pairs. The minor groove edge of the dC5 sugar ring is positioned over the plane of the displaced modified dG6 residue.

Solution Structure. A view normal to the helix axis and looking into the minor groove for the central d(T4-C5-[BP]-G6-C7-T8)·d(A15-G16-G17-A18) segment of the representative structure of the ensemble of six relaxation matrix refined structures of the (−)-*trans-anti*-[BP]dG·del 11/10-mer is shown in Figure 7A. The covalently linked benzo[*a*]pyrenyl moiety intercalates between intact Watson−Crick dC5·dG17 and dC7·dG16 base pairs and displaces the deoxyguanosine ring of [BP]dG6 into the minor groove (Figure 7A). The minor groove face of the sugar ring of dC5 is positioned over the deoxyguanosine base plane of [BP]dG6 which is directed toward the 5′-end of the modified strand and aligned approximately parallel to the helix axis. The intercalation site is wedge-shaped resulting in a shorter separation between the base planes of dG16 and dG17 on the deletion containing strand relative to the base planes of dC5 and dC7 on the modified strand (Figure 7A).

The long axis of the intercalated benzo[*a*]pyrenyl ring is approximately normal to the long axis of the flanking dC5·dG17 and dC7·dG16 base pairs with its benzylic ring positioned in the minor groove and the aromatic pyrenyl ring system extending into the major groove (Figure 7B). This intercalation orientation positions the pyrene ring over the Watson−Crick pairing edge of both flanking dG·dC base pairs (Figure 7B).

The benzylic ring of BP is in the distorted half-chair conformation with the BP(H9) and BP(H10) in pseudoequatorial orientations while the BP(H7) and BP(H8) adopt pseudoaxial orientations. The carcinogen-base linkage site for the [BP]dG6 residue is defined by the angles α' [dG6-(N^1)-dG6(C^2)-dG6(N^2)-BP(C^{10})] = 194 ± 9° and β' [dG6-(C^2)-dG6(N^2)-BP(C^{10})-BP(C^9)] = 95 ± 9° among the ensemble of six structures obtained from the relaxation matrix refinement of the (−)-*trans-anti*-[BP]dG·del 11/10-mer.

Some of the glycosidic torsion angles and sugar puckers for the d(T4-C5-[BP]G6-C7-T8)·d(A15-G16-G17-A18) segment of the (−)-*trans-anti*-[BP]dG·del 11/10-mer differ from those most common in B-DNA duplexes (Berman et al., 1992). The ensemble of six structures obtained from the relaxation matrix refinement was B-like except that the glycosidic torsion angles for [BP]dG6 and dC7, which are in the *anti* range, adopt unusual low values of 164.8 ± 10.0° and 185.5 ± 13.5°, respectively. The pseudorotation *P* values of dC5 and dC7 are 8.6 ± 23.3° and 346.1 ± 20.4°, respectively, which place these sugars in the C3′-*endo* and C2′-*exo* domain, respectively.

DISCUSSION

Spectral Quality. The exchangeable imino (Figure 2A) and non-exchangeable base and sugar proton resonances (Figure 2B) are well resolved for the (−)-*trans-anti*-[BP]-dG·del 11/10-mer. The adduct 11/10-mer adopts a single conformation on the basis of the proton spectra (Figure 2) and the absence of exchange peaks in the NOESY spectra.

NOE Patterns. The orientation of the intercalated benzo[*a*]pyrene ring between the flanking dG·dC base pairs in the solution structure of the (−)-*trans-anti*-[BP]dG·del 11/10-mer (Figure 7) is supported by both the experimental NOE and chemical shift data. Thus, the alignment of the C^{10}-C^{11}-C^{12}-containing long edge of the BP ring toward the d(C5-[BP]G6-C7) segment of the modified strand (Figure 7B) results in the observation of intermolecular NOEs between the BP(H10), BP(H11), and BP(H12) protons and the sugar protons of dC5, [BP]dG6, and dC7 which are satisfied in the solution structure (Table S2). This alignment requires the BP(H10) proton to be closer to the C7 sugar and the BP(H12) proton to be closer to the C5 sugar (Figure 7B), which is consistent with the experimental NOEs between these BP protons and the corresponding sugar H1′ protons (Table S2 and S3). The alignment of the C^4-C^5-C^6-containing long edge of the BP ring toward the d(G16−G17) segment of the deletion containing strand (Figure 7B) is supported by the observed NOEs between the BP(H3), BP(H4), BP(H5), and BP(H6) protons and the imino and sugar protons of dG16 and dG17 (Tables S2 and S3). The C^1-C^2-C^3 edge of the pyrenyl ring of BP is positioned in the major groove, while the C^7-C^8-C^9 edge of the benzylic ring of BP is positioned in the minor groove in the solution structure of the (−)-*trans-anti*-[BP]dG·del 11/10-mer (Figure 7B). The structural distortion resulting from base displacement of the deoxyguanosine of [BP]dG6 into the minor

groove should perturb the NOEs between DNA protons on adjacent residues in the d(C5-[BP]G6-C7)·d(G16-G17) segment centered about the pyrenyl intercalation site in the solution structure of the (−)-*trans-anti*-[BP]dG·del 11/10-mer. Sequential NOEs are absent between the H8 proton of [BP]dG6 and the sugar H1′, H2′, H2″, and H3′ protons of dC5 for the d(C5-[BP]G6) step. Weak to very weak sequential NOEs are observed between the H6 proton of dC7 and the sugar H1′, H2′, H2″, and H3′ protons of [BP]dG6 for the d([BP]G6-C7) step. The absence of an NOE between the H8 proton of [BP]dG6 and the H5 proton of dC7 for the purine (3′-5′) pyrimidine d([BP]G6-C7) step is consistent with the orthogonal arrangement of the modified dG6 and dC7 base planes in the adduct 11/10-mer.

The wedge-shaped intercalation site generated between the dC5·dG17 and dC7·dG16 base pairs is reflected in the 4.5 ± 0.5 Å separation between the H8 protons of dG16 and dG17 on the deletion containing strand and the 7.1 ± 0.6 Å separation between the H6 protons of dC5 and dC7 on the modification containing strand in the ensemble of six structures of the (−)-*trans-anti*-[BP]dG·del 11/10-mer (Figure 7A).

The modified deoxyguanosine is displaced into the minor groove with its plane positioned over the minor groove face of the sugar ring of C5 in the structure of the (−)-*trans-anti*-[BP]dG·del 11/10-mer (Figure 7A). This alignment is consistent with the very weak NOE observed between the H8 proton of [BP]dG6 and the minor groove H4′ proton of C5 (Figure S2, Supporting Information) observed for the adduct 11/10-mer.

Chemical Shift Patterns. The intercalated pyrenyl ring stacks primarily over the Watson−Crick edges of the dG16, dG17, and dC7 bases of the flanking dG·dC base pairs in the solution structure of the (−)-*trans-anti*-[BP]dG·del 11/10-mer. Consistent with this overlap geometry are the large upfield ring current shifts observed at the imino protons of dG16 (−1.35 ppm) and dG17 (−2.00 ppm), the amino protons of dC7 (−0.65, −1.05 ppm), and, to a lesser extent, the amino protons of dC5 (−0.18, −0.95 ppm) in the adduct 11/10-mer relative to the control 11/10-mer (Table S4). The pyrenyl ring also stacks over the H1′ proton of dC7 accounting for the large −1.60 ppm upfield shift. The H8 and H1′ protons of [BP]dG6 are shifted to low field by +0.24 and +0.58 ppm, respectively (Table S4), consistent with the modified deoxyguanosine being displaced into the minor groove in the solution structure of the adduct 11/10-mer (Figure 7A). The minor groove sugar H1′ and H2″ protons of dC5 are shifted to high field by −0.49 and −1.08 ppm, respectively (Table S4), consistent with the displaced modified deoxyguanosine ring stacking directly over the minor groove face of dC5 in the solution structure of the adduct 11/10-mer (Figure 7A).

The pyrenyl protons are also upfield-shifted in the adduct 11/10-mer relative to their unperturbed values in the 8.0−8.5 ppm chemical shift range (Figure 5). This reflects upfield ring current shifts from the flanking dG·dC base pairs which stack over the intercalated pyrenyl ring system. The BP-(H4) proton at 5.66 ppm stacks directly over the purine rings of the dG16 and dG17 (Figure 7B), consistent with its unusual upfield shift. The BP(H5) at 6.62 ppm, and, to a lesser extent, the BP(H3) proton at 6.78 ppm, stack over the periphery of the purine rings (Figure 7B) explaining their upfield shifts relative to other pyrenyl protons (Figure 5).

Comparison of First-Stage DUPLEX and Second-Stage X-PLOR Intensity Refined Structures. The key conformational features centered about the [BP]dG adduct positioned opposite a −1 deletion site are shared by both the first-stage DUPLEX and second-stage X-PLOR intensity refined structures of the (−)-*trans-anti*-[BP]dG·del 11/10-mer. This includes intercalation of the pyrenyl ring into the helix, the overlap of the pyrenyl ring with flanking base pairs and base displacement of the modified guanine into the minor groove. Further, the carcinogen−base linkage site torsion angles α′ [dG6(N^1)-dG6(C^2)-dG6(N^2)-BP(C^{10})] and β′ [dG6(C^2)-dG6(N^2)-BP(C^{10})-BP(C^9)] are 178° and 94°, respectively, for the lowest energy DUPLEX derived structure and are 194 ± 9° and 95 ± 9°, respectively, for the X-PLOR intensity refined structures. The discussion presented below will use the relaxation matrix refined structure of the (−)-*trans-anti*-[BP]-dG·del 11/10-mer (this study) for comparison with related DUPLEX based structures of (−)-*trans-anti*-[BP]dG·dC 11-mer duplex (de los Santos et al., 1992), (+)-*cis-anti*-[BP]-dG·del 11/10-mer (Cosman et al., 1994b) and (+)-*trans-anti*-[BP]dG·del 11/10-mer (Cosman et al., 1994a) published previously.

Different Conformations of the (−)-trans-anti-[BP]dG Adducts Opposite dC and a −1 Deletion Site. The solution structures of the central segment of the (−)-*trans-anti*-[BP]-dG·dC 11-mer duplex (de los Santos et al., 1992) and the (−)-*trans-anti*-[BP]dG·del 11/10-mer (this study) are shown in the same relative global orientation of the DNA in Figures 8A and 8B, respectively. The orientation of the [BP]dG residues are strikingly different in the two structures of the (−)-*trans-anti*-[BP]dG adducts opposite dC and opposite a −1 deletion site. The aromatic portion of the BP residue is positioned in the minor groove without base pair disruption and is directed toward the 3′-end of the modified strand when the adduct is positioned opposite dC (Figure 8A). However, the aromatic portion of the BP residue is intercalated into the helix with displacement of the modified deoxyguanosine into the minor groove when the adduct is positioned opposite a −1 deletion site (Figure 8B). Furthermore, one face of the aromatic ring system is exposed to solvent in the [BP]-dG·dC structure (Figure 8A), while it is intercalated between base pairs in the [BP]dG·del structure (Figure 8B). Thus, removing the partner dC residue to create a deletion site opposite the (−)-*trans-anti*-[BP]dG adduct results in a dramatic conformational change at the lesion site.

Similarity of (+)-cis-anti- and (−)-trans-anti-[BP]dG Adducts Opposite −1 Deletion Sites. The solution structures of the central segment of the (+)-*cis-anti*-[BP]dG·del 11/10-mer (Cosman et al., 1994b) and the (−)-*trans-anti*-[BP]-dG·del 11/10-mer (this study) are shown in the same relative orientation of the DNA in Figures 8C and 8B, respectively. We note a striking resemblance in the conformations of these two adducts, which have the same 10*R* absolute configuration at the BP(C^{10})-N^2-dG linkage site but have opposite orientations of the three hydroxyl groups at the chiral C^7, C^8, and C^9 positions. In both structures, the BP aromatic ring systems are intercalatively wedged into the helix between the two flanking dG·dC base pairs; the modified deoxyguanosines are displaced into the minor groove with their faces parallel to the helix axis and stacked over the minor groove face of the dC5 sugar ring. The benzylic ring of the BP residue is positioned in the minor groove in both structures, with the distal pyrenyl ring system positioned in

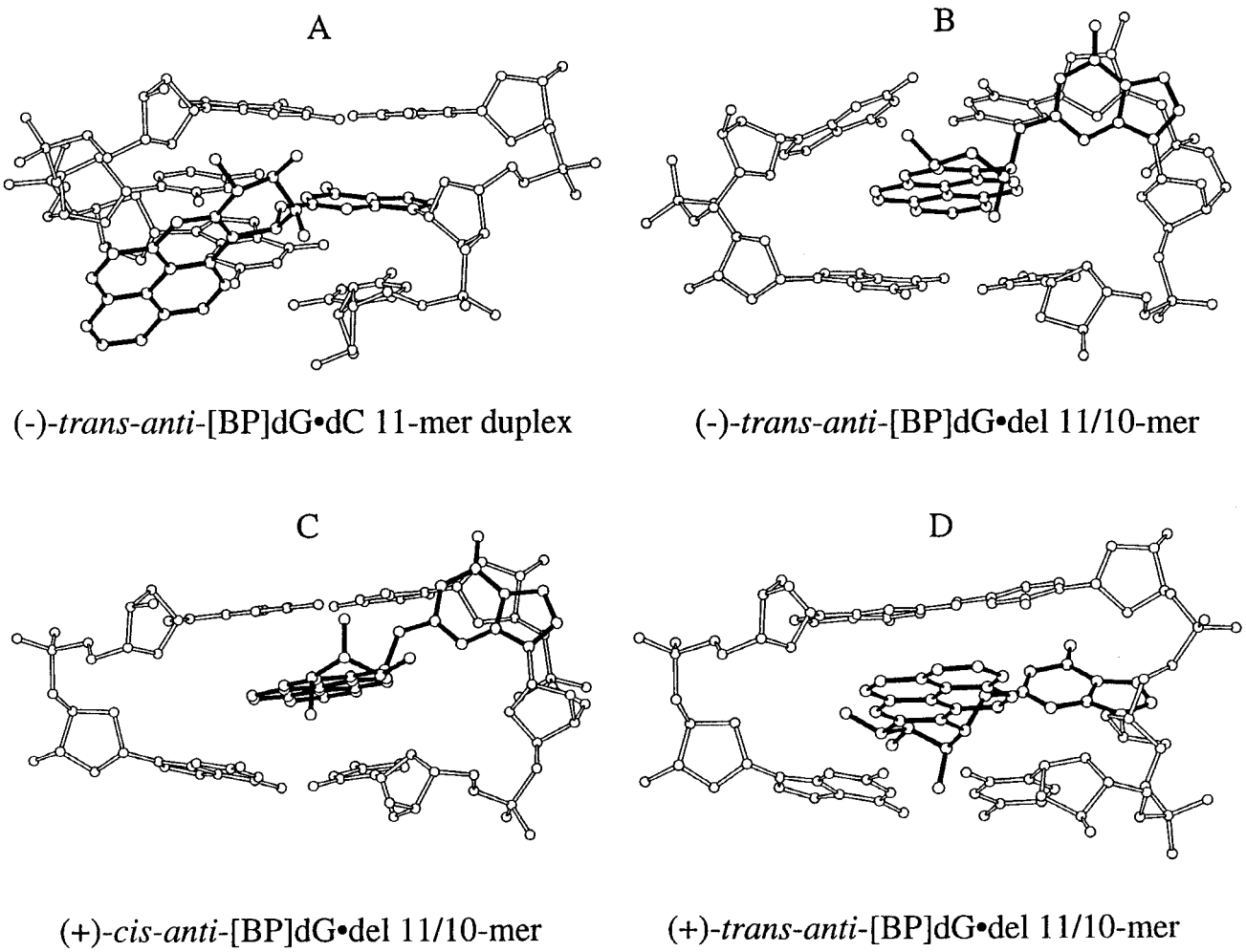

FIGURE 8: Views looking into the minor groove and normal to the helix axis for the solution structures of (A) the d(T4-C5-[BP]G6-C7-T8)·d(A15-G16-T17-G18-A19) segment of the (−)-*trans-anti*-[BP]dG·dC 11-mer duplex following DUPLEX refinement (de los Santos et al., 1992), as well as the d(T4-C5-[BP]G6-C7-T8)·d(A15-G16-G17-A18) segment of (B) the (−)-*trans-anti*-[BP]dG·del 11/10-mer following relaxation matrix refinement (this study), (C) the (+)-*cis-anti*-[BP]dG·del 11/10-mer following DUPLEX refinement (Cosman et al., 1994b) and (D) the (+)-*trans-anti*-[BP]dG·del 11/10-mer following DUPLEX refinement (Cosman et al., 1994a).

the major groove. The carcinogen−base linkage torsion angles α′ [dG6(N^1)-dG6(C^2)-dG6(N^2)-BP(C^{10})] for the (−)-*trans-anti*-[BP]dG·del 11/10-mer (194°) and the (+)-*cis-anti*-[BP]dG·del 11/10-mer (160°) are similar as are the carcinogen−base linkage torsion angles β′ [dG6(C^2)-dG6(N^2)-BP(C^{10})-BP(C^9)] for the (−)-*trans-anti*-[BP]dG·del 11/10-mer (95°) and the (+)-*cis-anti*-[BP]dG·del 11/10-mer (91°).

Opposite Orientations of the (+)-trans-anti- and the (−)-trans-anti-[BP]dG Adducts Opposite −1 Deletion Sites. The solution structures of the central segments of the 10*S* (+)-*trans-anti*-[BP]dG·del 11/10-mer (Cosman et al., 1994a) and the 10*R* (−)-*trans-anti*-[BP]dG·del 11/10-mer (this study) are shown in the same relative global orientation of the DNA in Figures 8D and 8B, respectively. These two adducts have the opposite absolute configuration at the BP(C^{10}) linkage site. The aromatic portion of the BP residue intercalates between intact Watson−Crick dC5·dG17 and dC7·dG16 base pairs which generate a wedge-shaped intercalation site with base displacement of the modified deoxyguanosine in both structures. The carcinogen−base α′ torsion angles are similar for the (+)-*trans-anti*-[BP]dG adduct (α′ = 138°) and (−)-*trans-anti*-[BP]dG adduct (α′ = 194°) positioned opposite −1 deletion sites. By contrast, the carcinogen-base β′ torsion angles are very different for the (+)-*trans-anti*-[BP]dG adduct (β′ = 263°) and (−)-*trans-anti*-[BP]dG adduct (β′ = 95°) positioned opposite −1 deletion sites, indicative of a nearly 180° difference between the two stereoisomers (Figures 8D and 8B, respectively). This reflects the striking opposite orientation of the pyrenyl moiety, by an approximately 180° rotation about the helix axis, in these two adducts derived from chiral pairs of diol epoxides.

The benzylic ring of the BP residue and the attached base displaced deoxyguanosine are positioned in the major groove with the distal pyrene rings in the minor groove in the case of the (+)-*trans-anti*-[BP]dG adduct stereoisomer opposite a −1 deletion site (Figure 9A). By contrast, the benzylic ring is in the minor groove with the distal pyrenyl ring in the major groove for the (−)-*trans-anti*-[BP]dG adduct positioned opposite a −1 deletion site (Figure 9B). The modified deoxyguanosine stacks over the major groove base protons (H5 and H6) of dC5 in the (+)-*trans-anti*-[BP]dG adduct (Figure 8D) and stacks over the minor groove face sugar protons (H1′, H2″, and H4′) of dC5 in the (−)-*trans-anti*-[BP]dG adduct (Figure 8B) opposite −1 deletion sites.

The Theme of Opposite Orientations of DNA Adducts Derived from Diol Epoxides of Opposite Chiralities. Opposite orientations of the PAH residues relative to the covalently attached purine residues in adducts derived from chiral pairs of PAH diol epoxide enantiomers is a recurring

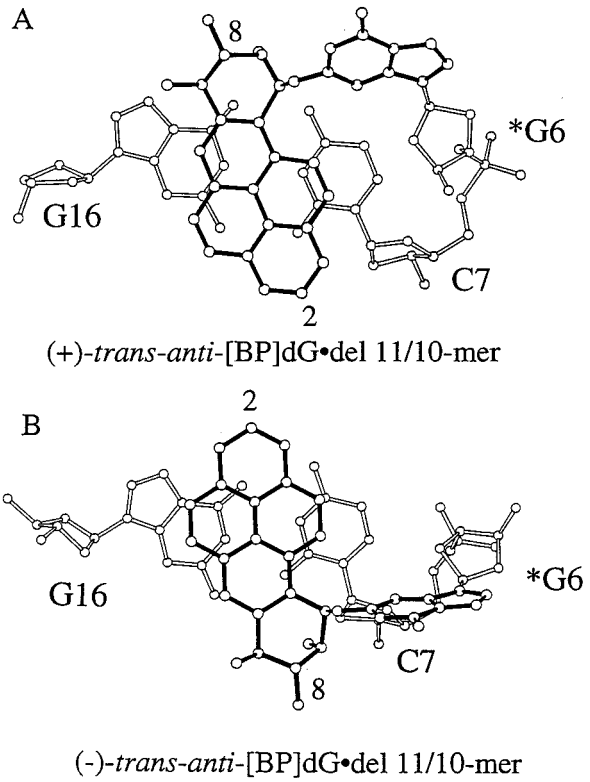

FIGURE 9: Views looking down the helix axis for the d([BP]G6-C7)·dG16 segments in the solution structures obtained by molecular mechanics calculations using DUPLEX of (A) the (+)-*trans-anti*-[BP]dG·del 11/10-mer and (B) the (−)-*trans-anti*-[BP]dG·del 11/10-mer, showing the opposite orientations of the [BP]dG rings relative to major/minor grooves at intercalation sites. The benzylic ring is positioned in the major groove for the (+)-*trans-anti*-[BP]-dG adduct in (A) and in the minor groove for the (−)-*trans-anti*-[BP]dG adduct in (B) at the 11/10-mer level.

theme that has been noted in a number of different examples [reviewed in Geacintov et al. (1997)]. These include (1) the minor groove (+)- and (−)-*trans-anti*-[BP]-N^2-dG adducts opposite dC (Cosman et al., 1992; de los Santos et al., 1992), (2) the base-displaced intercalative conformations of (+)- and (−)-*cis-anti*-[BP]-N^2-dG opposite dC (Cosman et al., 1993a, 1996), (3) the (+)-*cis-anti*- (Cosman et al., 1994b), (+)-*trans-anti*- (Cosman et al., 1994a), and (−)-*trans-anti*-[BP]-N^2-dG adducts (this work) opposite −1 deletion sites, (4) (+)- and (−)-*trans-anti*-[BPh]-N^6-dA adducts (derived from fjord region benzo[*c*]phenanthrene diol epoxide enantiomers) opposite dT (Cosman et al., 1993b, 1995) and (5) *anti*-[BP]-N^6-dA adducts in several different sequence contexts (Schurter et al., 1995a,b; Yeh et al., 1995; Zegar et al., 1996b). Similar characteristics are exhibited by the *R* and *S* N^6-dA (Feng et al., 1995, 1996) and N^2-dG adducts (Zegar et al., 1996a) derived from styrene oxide. These differing conformational themes with the common feature of opposite orientations associated with opposite linkage site *R* and *S* absolute configurations appear to be general and are independent of specific conformational type, nature of the modified base, or the nature of the PAH residue. Such profound effects of opposite absolute configurations of the covalently bound PAH residues could be associated with different patterns of response to DNA repair, transcription, and replication enzymes that could account for the observed differences in the biological activities of chiral pairs of PAH diol epoxide stereoisomers.

Slipped Frameshift Intermediates and DNA Replication. The NMR solution structures of the three deletion 11/10-mers, i.e. sequences lacking the normal partner dC residues in the complementary strand opposite (+)-*trans-anti*-, (−)-*trans-anti*-, and (+)-*cis-anti*-[BP]dG lesions, reveal that all three form stable −1 deletion 11/10-mers at ambient temperatures. Indeed, the melting points (T_m) of the −1 deletion 11/10-mers at 10 μM concentrations increase by 6, 25, and 14 °C on proceeding from the control 11/10-mer to the (+)-*trans-anti*-, (+)-*cis-anti*-, and (−)-*trans-anti*-[BP]dG adduct containing 11/10-mers, respectively (Ya et al., 1994). Other examples of stable −1 and −2 deletion duplexes, are the 2-aminofluorene-C^8-dG adducts which also manifest a base-displaced intercalation conformation, as well as thermal stabilization of the deletion duplexes by the intercalated 2-aminofluorene residue (Mao et al., 1995a,b). Thus, the shared conformational feature of base-displaced intercalation, with the stabilizing stacking interactions between the carcinogen residues and the flanking bases, seem to account for the remarkable duplex stabilization in these polynuclear aromatic carcinogen-modified deletion duplexes. Thermal stabilization of deletion duplexes with modification by 2-acetylaminofluorene (AAF) has also been observed (Garcia et al., 1993; Milhe et al., 1996).

Stalling of the polymerases at bulky lesions, could allow for the formation of misaligned primer−template intermediates that could result in frameshift mutations during DNA replication if the sequence is appropriate (Streisinger et al., 1966; Kunkel et al., 1990; Belguise-Valladier & Fuchs, 1991; Lambert et al., 1992; Shibutani & Grollman, 1993; Napolitano et al., 1994). A base-displaced intercalative structure of the type observed in our modified deletion duplexes might well stabilize such a slipped frameshift intermediate. The −1 deletion duplex which is the focus of this study, represents the structure of a primer/template complex in which the primer has been extended by five bases beyond the site of the lesion and has suffered a −1 deletion mutation in the process. Our results with three stereoisomeric BPDE-modified deletion duplexes [this work and Cosman et al. (1994a,b)], indicate normal Watson−Crick base pairing and stacking on the 5′-side of the modified strand with a −1 deletion in the unmodified (primer) strand, suggesting that further DNA synthesis can proceed normally, thus fixing the −1 frameshift mutation.

Coordinates Deposition. The coordinates of the (−)-*trans-anti*-[BP]dG·del 11/10-mer are being deposited in the Protein Data Base, Brookhaven National Laboratory, Upton, New York 11923, from whom copies can be obtained (accession code, 1AXL).

SUPPORTING INFORMATION AVAILABLE

Four tables listing exchangeable and non-exchangeable proton chemical shifts for the entire (−)-*trans-anti*-[BP]dG·del 11/10-mer, a comparison of intermolecular NOEs with distances observed in the refined structures and proton chemical shift differences on adduct formation, and five figures showing the structures of the four stereoisomeric BPDE adducts, an expanded NOESY contour plot in D_2O, phosphorus spectra, the superposition of five structures that best fit the NMR data obtained by molecular mechanics calculations using DUPLEX, and the final unrestrained energy minimized structure obtained by molecular mechanics

calculations using DUPLEX (11 pages). Ordering information is given on any current masthead page.

REFERENCES

Altona, C., & Sundaralingam, M. (1972) *J. Am. Chem. Soc. 94*, 8205−8212.

Belguise-Valladier, P., & Fuchs, R. P. P. (1991) *Biochemistry 30*, 10091−10100.

Berman, H. M., Olson, W. K., Beveridge, D. L., Westbrook, J., Gelbin, A., Demeny, T., Hsieh, S. H., Srinivasan, A. R., & Schneider, B. (1992) *Biophys. J. 63*, 751−759.

Brookes, P., & Osborne, M. R. (1982) *Carcinogenesis 3*, 1223−1226.

Buening, M. K., Wislocki, P. G., Levin, W., Yagi, H., Thakker, D. R., Akagi, H., Koreeda, M., Jerina, D. M., & Conney, A. H. (1978) *Proc. Natl. Acad. Sci. U.S.A. 75*, 5358−5361.

Cheng, S. C., Hilton, B. D., Roman, J. M., & Dipple, A. (1989) *Chem. Res. Toxicol. 2*, 334−340.

Conney, A. H. (1982) *Cancer Res. 42*, 4875−4917.

Cosman, M., Ibanez, V., Geacintov, N. E., & Harvey, R. G. (1990) *Carcinogenesis 11*, 1667−1672.

Cosman, M., de los Santos, C., Fiala, R., Hingerty, B. E., Ibanez, V., Margulis, L. A., Live, D., Geacintov, N. E., Broyde, S., & Patel, D. J. (1992) *Proc. Natl. Acad. Sci. U.S.A. 89*, 1914−1918.

Cosman, M., de los Santos, C., Fiala, R., Hingerty, B. E., Ibanez, V., Luna, E., Harvey, R. G., Geacintov, N. E., Broyde, S., & Patel, D. (1993a) *Biochemistry 32*, 4145−4155.

Cosman, M., Fiala, R., Hingerty, B. E., Laryea, A., Lee, H., Harvey, R. G., Amin, S., Geacintov, N. E, Broyde, S., & Patel, D. J. (1993b) *Biochemistry 32*, 12488−12497.

Cosman, M., Fiala, R., Hingerty, B. E., Amin, S., Geacintov, N. E., Broyde, S., & Patel, D. J. (1994a) *Biochemistry 33*, 11507−11517.

Cosman, M., Fiala, R., Hingerty, B. E., Amin, S., Geacintov, N. E., Broyde, S., & Patel, D. J. (1994b) *Biochemistry 33*, 11518−11527.

Cosman, M., Laryea, A., Fiala, R., Hingerty, B. E., Amin, S., Geacintov, N. E., Broyde, S., & Patel, D. J. (1995) *Biochemistry 34*, 1295−1307.

Cosman, M., Hingerty, B. E., Luneva, N., Amin, S., Geacintov, N. E., Broyde, S., & Patel, D. J. (1996) *Biochemistry 35*, 9850−9863.

de los Santos, Cosman, M., Hingerty, B. E., Ibanez, V., Margulis, L. A., Geacintov, N. E., Broyde, S., & Patel, D. J. (1992) *Biochemistry 31*, 5245−5252.

Feng, B., Zhou, L., Passarelli, Harris, C. M., Harris, T. M., & Stone, M. P. (1995) *Biochemistry 34*, 14021−14036.

Feng, B., Gorin, A., Voehler, M., Zhou, L., Passarelli, Harris, C. M., Harris, T. M., & Stone, M. P. (1996) *Biochemistry 35*, 7316−7329.

Feng, B., Kolbanovskiy, A., Hingerty, B. E., Geacintov, N. E., Broyde, S., & Patel, D. J. (1997) *Biochemistry 36*, xxx−xxx (accompanying paper in this issue).

Fountain, M. A., & Krugh, T. R. (1995) *Biochemistry 34*, 3152−3161.

Garcia, A., Lambert, I. B., & Fuchs, R. P. P. (1993) *Proc. Natl. Acad. Sci. U.S.A. 90*, 5989−5993.

Geacintov, N. E., Cosman, M., Hingerty, B. E., Amin, S., Broyde, S., & Patel, D. J. (1997) *Chem. Res. Toxicol. 10*, 111−146.

Harvey, R. G., *Polycyclic Aromatic Hydrocarbons: Chemistry and Carcinogenicity*, Cambridge University Press, Cambridge, U.K., 1991.

Hingerty, B. E., Figueroa, S., Hayden, T., & Broyde, S. (1989) *Biopolymers 28*, 1195−1222.

Kumar, A, Ernst, R. R., & Wuthrich, K. (1980) *Biochem. Biophys. Res. Commun. 95*, 1−6.

Kunkel, T. A. (1990) *Biochemistry 29*, 8003−8011.

Lambert, I. B., Napolitano, R. L., & Fuchs, R. P. (1992) *Proc. Natl. Acad. Sci. U.S.A. 89*, 1310−1314.

Majumdar A., & Hosur, R. V. (1992) *Prog. NMR Spectrosc. 24*, 109−158.

Mao, B., Cosman, M., Hingerty, B. E., Broyde, S., & Patel, D. J. (1995a) *Biochemistry 34*, 6226−6238.

Mao, B., Hingerty, B. E., Broyde, S., & Patel, D. J. (1995b) *Biochemistry 34*, 16641−16653.

Meehan, T., & Straub, K. (1979) *Nature 277*, 410−412.

Milhe, C., Fuchs, R. P. P., & Lefevre, J.-F. (1996) *Eur. J. Biochem. 235*, 120−127.

Moriya, M., Spiegel, S., Fernandes, A., Amin, S., Liu, T.-M., Geacintov, N. E., & Grollman, A. P. (1996) *Biochemistry 35*, 16646−16651.

Napolitano, R. L., Lambert, I. B., & Fuchs, R. P. (1994) *Biochemistry 33*, 1311−1315.

Neidle, S., Subiah, A., Kuroda, R., & Cooper, C. S. (1982) *Cancer Res. 42*, 3716−3768.

Patel, D. J., Shapiro, L., & Hare, D. (1987) *Annu. Rev. Biophys. Biophys. Chem. 16*, 423−454.

Schurter, E. J., Yeh, H. J. C., Sayer, J. M., Lakshman, M. K., Yagi, H., Jerina, D. M., & Gorenstein, D. G. (1995a) *Biochemistry 34*, 1364−1375.

Schurter, E. J., Sayer, J. M., Oh-hara, T., Yeh, H. C. J., Yagi, H., Luxon, B. A., Jerina, D. M., & Gorenstein, D. G. (1995b) *Biochemistry 34*, 9009−9020.

Shibutani, S., & Grollman, A. P. (1993) *J. Biol. Chem. 268*, 11703−11710.

Singer, B., & Grunberger, D. (1983) *Molecular Biology of Mutagens and Carcinogens*, Plenum Press, New York.

Slaga, T. J., Bracken, W. J., Gleason, G., Levin, W., Yagi, H., Jerina, D. M., & Conney, A. H. (1979) *Cancer Res. 39*, 67−71.

Streisinger, G., Okada, Y., Emrich, J., Newton, J., Tsugita, A., Terzaghi, F., & Inouye, M. (1966) *Cold Spring Harbor Symp. Quant. Biol. 31*, 77−84.

van der Ven, F. J., & Hilbers, C. W. (1988) *Eur. J. Biochem. 178*, 1−38.

Wei, S.-J. C., Chang, R. L., Hennig, E., Cui, X. X., Merkler, K. A., Wong, C.-Q., Yagi, H., & Conney, A. H. (1994) *Carcinogenesis 15*, 1729−1735.

Wood, A. W., Chang, R. L., Levin, W., Yagi, H., Thakker, D. R., Jerina, D. M., & Conney, A. H. (1977) *Biochem. Biophys. Res. Commun. 77*, 1389−1396.

Ya, N.-Q., Smirnov, S., Cosman, M., Bhanot, S., Ibanez, V., & Geacintov, N. E. (1994) In: *Structural Biology: The State of the Art*, Proceedings of the 8th Conversation Sarma, R. H., & Sarma, M. H., Eds.) Vol. 2, pp 349−366, Adenine Press, Schenectady, NY.

Yeh, H. J. C., Sayer, J. M., Liu, X., Altieri, A. S., Byrd, R. A., Lakshman, M. K., Yagi, H., Schurter, E. J., Gorenstein, D. G., & Jerina, D. M. (1995) *Biochemistry 34*, 13570−13581.

Zegar, I. S., Setayesh, F. R., DeCorte, B. L., Harris, C. M., Harris, T. M., & Stone, M. P. (1996a) *Biochemistry 35*, 4334−4348.

Zegar, I. S., Kim, S. J., Johansen, T. N., Harris, C. M., Harris, T. M., & Stone, M. P. (1996b) *Biochemistry 35*, 6212−6224.

BI970070R